Article

目下而上的克级石墨烯的合成
Gram-scale bottom-up flash graphene synthesis

https://doi.org/10.1038/s41586-020-1938-0

接收日期：2019年5月28日
Received: 28 May 2019

接受日期：2019年10月22日
Accepted: 22 October 2019

在线发布：xx xx xxxx
Published online: 27 January 2020

Duy X. Luong[1,2], Ksenia V. Bets[3], Wala Ali Algozeeb[2], Michael G. Stanford[2], Carter Kittrell[2], Weiyin Chen[2], Rodrigo V. Salvatierra[2], Muqing Ren[2], Emily A. McHugh[2], Paul A. Advincula[2], Zhe Wang[2], Mahesh Bhatt[4], Hua Guo[3], Vladimir Mancevski[2], Rouzbeh Shahsavari[4,5]*, Boris I. Yakobson[2,3,6]* & James M. Tour[2,3,6]*

大多数大块石墨烯是通过自上而下的方法生产的, 即剥落石墨, 这种方法通常需要大量的高能混合、剪切、超声波或电化学处理的溶剂[1-3].
Most bulk-scale graphene is produced by a top-down approach, exfoliating graphite, which often requires large amounts of solvent with high-energy mixing, shearing, sonication or electrochemical treatment[1–3]. Although chemical oxidation of graphite to graphene oxide promotes exfoliation, it requires harsh oxidants and leaves the graphene with a defective perforated structure after the subsequent reduction step[3,4]. Bottom-up synthesis of high-quality graphene is often restricted to ultrasmall amounts if performed by chemical vapour deposition or advanced synthetic organic methods, or it provides a defect-ridden structure if carried out in bulk solution[4–6]. Here we show that flash Joule heating of inexpensive carbon sources—such as coal, petroleum coke, biochar, carbon black, discarded food, rubber tyres and mixed plastic waste—can afford gram-scale quantities of graphene in less than one second. The product, named flash graphene (FG), after the process used to produce it, shows turbostratic arrangement (that is, little order) between the stacked graphene layers. FG synthesis uses no furnace and no solvents or reactive gases. Yields depend on the carbon content of the source; when using a high-carbon source, such as carbon black, anthracitic coal or calcined coke, yields can range from 80 to 90 per cent with carbon purity greater than 99 per cent. No purification steps are necessary. Raman spectroscopy analysis shows a low-intensity or absent D band for FG, indicating that FG has among the lowest defect concentrations reported so far for graphene, and confirms the turbostratic stacking of FG, which is clearly distinguished from turbostratic graphite. The disordered orientation of FG layers facilitates its rapid exfoliation upon mixing during composite formation. The electric energy cost for FG synthesis is only about 7.2 kilojoules per gram, which could render FG suitable for use in bulk composites of plastic, metals, plywood, concrete and other building materials.

尽管石墨化学氧化为氧化石墨烯会促进剥落, 但它需要苛刻的氧化剂, 并在随后的还原步骤3,4后使石墨烯具有缺陷的穿孔结构.

如果采用化学气相沉积或先进的有机合成方法进行自下而上的高质量石墨烯合成, 则通常仅限于极少量的石墨烯, 如果采用大量溶液4-6进行, 则石墨烯具有无缺陷的结构.

在这里, 我们表明, 对廉价的碳源, 如煤、石油焦、生物炭、炭黑、废弃食品、橡胶轮胎和混合塑料废料进行闪光焦耳加热, 可以在不到一秒钟的时间内提供克级数量的石墨烯.

该产品以其生产工艺命名为闪光石墨烯(flash graphene, FG), 它显示了层叠石墨烯层之间的涡轮层状排列(即小的有序).

FG合成不使用熔炉, 也不使用溶剂或反应气体. 产量取决于碳源的含碳量；当使用炭黑、无烟煤或煅烧焦炭等高碳源时, 产量可在80%至90%之间, 碳纯度大于99%.

这个方法无需净化步骤. 拉曼光谱分析显示FG具有低强度的或消失的D带, 表明FG是迄今为止报道的石墨烯缺陷浓度最低的材料之一, 证实了FG的涡轮层堆积, 这与涡轮层石墨有明显区别.

FG层的无序取向有利于其在复合材料形成过程中混合后的快速剥落.

FG合成的电能成本仅为每克7.2千焦耳, ,可使FG适用于塑料、金属、胶合板、混凝土和其他建筑材料的大块复合材料.

在闪光焦耳加热(FJH)过程中, 非晶态导电碳粉在两个电极之间的石英或陶瓷管中被轻轻压缩(图1a, 补充图1).

该系统可以在大气压下, 或在轻度真空(~10毫米汞柱)下, 以便于放气.

电极可以是铜、石墨或任何导电耐火材料, 它们松散地嵌入石英管中, 以便在FJH上放气.

电容器组的高压放电使碳源在不到100毫秒的时间内达到3000 K以上的温度, 有效地将非晶态碳转化为涡轮层FG.

在高分辨率透射电子显微镜(HR-TEM)分析(图1b, c)中, FG的错向层显示出预期的莫尔条纹, 而从废咖啡渣中提取的FG也显示出六角形单层石墨烯(图1d).

利用拉曼光谱可以快速鉴定出高质量的石墨烯,炭黑生成的FG(CB-FG)具有强烈的二维峰.

从图1e中CB-FG的Raman图谱可以看出, 在许多位置, 相对于G带(I2D/G)的2D带的强度大于10.

D带的极低强度表明这些FG产品的缺陷浓度很低, 这有助于2D带的变大.

因此, CB-FG的异常高I2D/G=17(图1e)是迄今为止报道的任何形式石墨烯的最高值, 并且可能是闪蒸过程中达到的极端温度的结果, 闪蒸过程从体系中释放出非碳元素.

此外, TS1和TS2分别在约1886cm -1和约2031cm -1处的两个峰值, 证实了FG的涡轮层性质(补充图2,3).

这在补充资料和补充表1[11], 12中有广泛讨论.

FG的X射线衍射(XRD)图显示一个清晰的(002)峰, 表明非晶碳石墨化成功.

[1]Applied Physics Program, Rice University, Houston, TX, USA. [2]Department of Chemistry, Rice University, Houston, TX, USA. [3]Department of Materials Science and NanoEngineering, Rice University, Houston, TX, USA. [4]C-Crete Technologies, Stafford, TX, USA. [5]Department of Civil and Environmental Engineering, Rice University, Houston, TX, USA. [6]Smalley-Curl Institute and the NanoCarbon Center, Rice University, Houston, TX, USA. *e-mail: rouzbeh@ccretetech.com; biy@rice.edu; tour@rice.edu

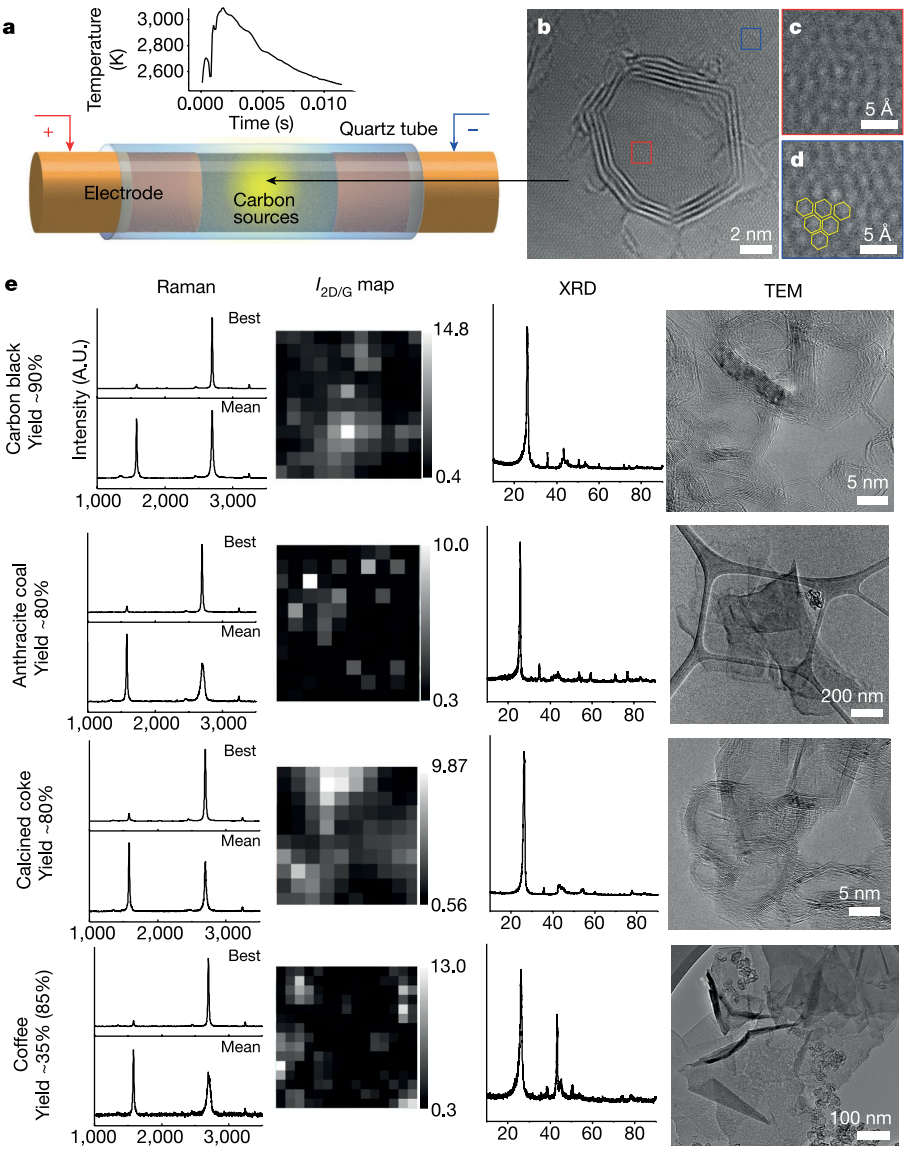

图1：由各种碳源合成的FG. a.FJH过程的示意图

Fig. 1 | FG synthesized from various carbon sources. a, Schematic of the FJH process, and plot of the temperature rise versus time during flashing (inset). 和闪蒸过程中的温升与时间的关系图(插图).
b–d, HR-TEM image of CB-FG on top of a single layer of coffee-derived FG. b-d, 在单层咖啡衍生FG上的CB-FG的HR-TEM图像.
e, Characterization results, including Raman spectra (showing the best and the mean obtained spectra), XRD spectra and TEM images for FG derived from various carbon sources. The coffee-derived FG is made from used coffee grounds; the smaller graphene particles within large graphene sheets come from the carbon black conductive additive. Each pixel in the Raman mapping is 4 μm^2, using a 50× magnification. All Raman samples were prepared from the powdered product after FJH; the samples were not exposed to the solvent before Raman analysis. Coffee is about 40% carbon, so the yield based on the starting carbon content is ~85%. The sample size for the mean Raman spectrum is 10. e.表征结果，包括拉曼光谱(显示了最佳和平均获得的光谱)、X射线衍射谱和TEM图像. 咖啡衍生的FG是由用过的咖啡渣制成的；大石墨烯片中较小的石墨烯颗粒由炭黑导电添加剂制成. 使用50倍放大率，拉曼图谱中的每个像素为4 μm^2，所有拉曼样品均由闪后的粉末产品制备；在拉曼分析之前，样品未暴露于溶剂中. 咖啡含碳量约为40%，以起始含碳量计算，产率约为85%. 平均拉曼光谱的样本量为10.

which corresponds to an interlayer spacing of l_c = 3.45 Å. This spacing is larger than that in a typical Bernal (AB-stacked) graphite, 3.37 Å, indicating the expanded and turbostratic structure of FG. The (002) peak was found to be unsymmetric, with a tail at small angles, which further suggests the turbostratic nature of FG[13]. The flash process is fast enough to prevent AB stacking. CB-FG has a surface area of ~295 m^2 g^{-1} with pore size <9 nm, as measured by Brunauer–Emmett–Teller analysis (Supplementary Fig. 4). Calcined petroleum coke (CPC) also works well for conversion to CPC-FG (Fig. 1e, Supplementary Table 2) which has a similar nanostructure to that of CB-FG. Together with carbon black, CPC is listed as a non-graphitized carbon source (Supplementary Table 3)[14]. The average size of CB-FG and CPC-FG is ~13 nm and ~17 nm, respectively (Supplementary Figs. 5, 6). The yield of the FJH process is as high as 80% to 90% from high-carbon sources such as carbon black, calcine coke or anthracite coal, and

相当于层间距l_c=3.45 Å，这种间距比典型的Bernal(AB堆积)石墨3.37的间距大，表明FG具有膨胀和涡轮层状结构. (002)峰是不对称的，在小角度有一个尾巴，这进一步表明了FG的涡轮层的性质. 闪光过程足够快，以防止AB堆叠. 根据Brunauer-Emmett-Teller分析(补充图4)，CB-FG的表面积约为295 m2 g -1，孔径小于9 nm. 煅烧石油焦(CPC)也能很好地转化为CPC-FG(图1e，补充表2)，后者具有与CB-FG相似的纳米结构. 与炭黑一起，CPC被列为非石墨化碳源(补充表3)14. CB-FG和CPC-FG的平均尺寸分别为~13nm和~17nm(补充图. FJH工艺的高碳产率高达80%～90%

它们转换所需的电能约为7.2 kJ g -1(补充信息).

the electric energy needed for their conversion is ~7.2 kJ g^{-1} (Supplementary Information).

In the case of coffee grounds, the used grounds were mixed with 5 wt% carbon black to increase its conductivity—alternatively, we could use 2–5 wt% FG from a previous run as the conductive additive. Coffee grounds, being predominantly carbohydrate, are ~40% carbon. Hence, the yield of graphene of ~35% (Fig. 1e) would be ~85% conversion of the coffee carbon content into graphene, whereas the heteroatoms sublime out at these reaction temperatures (≥3,000 K). Anthracite can be sufficiently conductive to be used in the FJH reactor, but better results were obtained by adding 5 wt% carbon black. Although a black FG powder is produced regardless of the starting material, FG from graphitizing carbons—such as from used coffee grounds (C-FG) and anthracite coal (A-FG) (see Supplementary Information for definitions of graphitizing and non-graphitizing carbons; see also Supplementary Table 3)—has

在咖啡渣的情况下，使用的咖啡渣与5 wt%的炭黑混合以增加其导电性，或者，我们可以使用以前运行的2-5 wt%的FG作为导电添加剂. 咖啡渣主要是碳水化合物，含碳量约为40%. 因此，约35%(图1e)的石墨烯的产率将是咖啡碳含量转化为石墨烯的约85%，而杂原子在这些反应温度(>3000k)下升华. 无烟煤具有足够的导电性，可用于FJH反应器，但加入5%的炭黑可获得较好的效果. 尽管黑FG粉末的生产与原料无关，但FG来自石墨化碳，例如来自旧咖啡渣(C-FG)和无烟煤(a-FG)(石墨化的定义见补充信息)，具有CB-FG的不同形态.

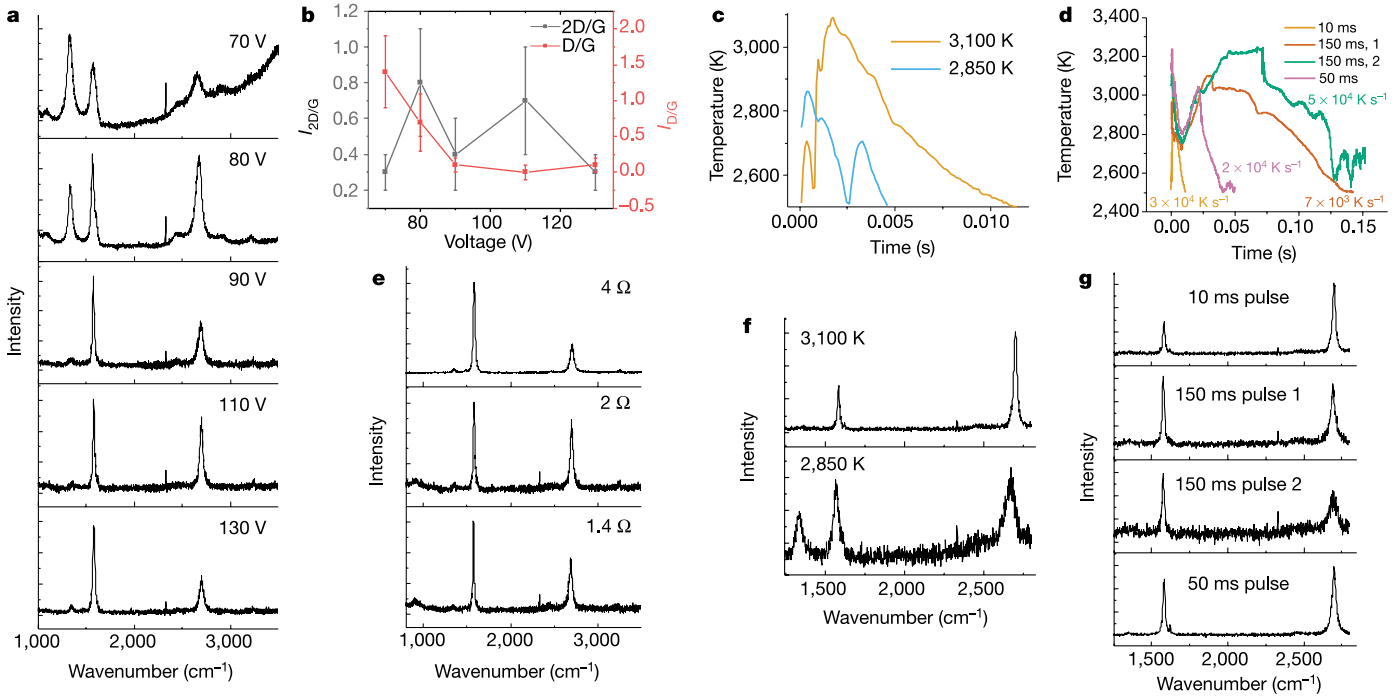

图2 | FJH关键参数. a,CB-FG的拉曼光谱随闪蒸电压的增加(从上到下). b,不同闪蒸电压下CB-FG的I2D/G和ID/G比值. c,CB-FG在不同温度下反应的时间-温度曲线. d,CB-FG在不同闪蒸时间下反应的时间-温度曲线. e,拉曼光谱

Fig. 2 | FJH critical parameters. **a**, Raman spectra of CB-FG with increasing flashing voltage (top to bottom). **b**, $I_{2D/G}$ and $I_{D/G}$ ratios of CB-FG at different flashing voltages. The bars represent 1 s.d. ($n = 10$). **c**, Time–temperature graph of CB-FG reacted at different temperatures. The temperature is regulated by the flashing voltage. **d**, Time–temperature graph of CB-FG reacted at different flashing durations. The flashing duration is regulated by the sample compression between the electrodes, which affects the sample conductivity. The numbers within the plot represent cooling rates. **e**, Raman spectra of CB-FG at different compression ratios. Higher compression provides lower resistance to the sample. **f**, Raman spectra of the CB-FG samples shown in **c**. **g**, Raman spectra of the CB-FG samples shown in **d**. The 150-ms pulses 1 and 2 have similar duration but different cooling rates, as shown in **d**. All Raman spectra in the figure were taken at low magnification (5×) to obtain a mean spectrum of the sample from 10 spectra.

different morphologies from CB-FG. Graphitizing carbons produce larger graphene sheets (Supplementary Fig. 7). XRD analysis of C-FG shows, in addition to the dominant (002) peak at 26.0°, a sharp (100) peak at $2\theta = 42.5°$, which is associated with the in-plane interatomic spacing (Fig. 1e). The narrow full width at half-maximum of the (100) peak suggests larger in-plane sheet sizes relative to FG formed from some of the other starting materials. HR-TEM reveals folded graphene sheets in A-FG and C-FG (Fig. 1e) with an average size of 0.5 μm and 1.2 μm (Supplementary Fig. 7), respectively, similar to the size of graphene sheet obtained by exfoliation of graphite[3,15,16]. Selected-area electron diffraction measurements on these samples show both monolayer and turbostratic graphene (Supplementary Figs. 8–10).

Other carbons that are abundant, renewable or waste-sourced can be used, such as charcoal, biochar, humic acid, keratin (human hair), lignin, sucrose, starch, pine bark, olive oil soot, cabbage, coconut, pistachio shells, potato skins, rubber tyres and mixed plastic (Supplementary Fig. 11, Supplementary Table 4), including polyethylene terephthalate (PET or PETE), high- or low-density polyethylene, polyvinyl chloride, polypropylene and polyacrylonitrile. When converting synthetic polymers into FG, the non-carbon atoms sublime out as small molecules, leading to a very-high-carbon-content product, as shown here. However, polymer and rubber depolymerization can also ensue to afford oligomers that sublime before conversion; therefore, it is more economical to use a pyrolysis product where the volatiles are first industrially removed for fuel sources[17] and the residual carbon is converted into FG. This was demonstrated here with rubber-tyre-derived carbon black (Supplementary Fig. 11, Supplementary Tables 2, 4). None of these FG processes was optimized. Optimization was performed only on CB-FG, as described below. The FJH process can provide a facile route to convert these waste products into FG, a potential high-value building-composite additive[18–21].

The graphene $I_{2D/G}$ is optimized by adjusting the sample compression between the electrodes (which affects sample conductivity), the capacitor voltage and the switching duration to control the temperature and duration of the flash (Fig. 2a–g). Increasing the voltage will increase the temperature of the process. The temperature is estimated by fitting the black-body radiation spectrum in the 600–1,100 nm emission (Supplementary Fig. 12). We investigated the quality of CB-FG using Raman spectroscopy at low magnification (see Methods) by varying the time and temperature in the FG synthesis process. At <90 V and <3,000 K, FG has a high D peak, indicating a defective structure (Fig. 2a–c, f). By increasing the voltage output, CB-FG is formed at 3,100 K, which has a low number of defects and almost no D band in the Raman spectrum. Therefore, 3,000 K is a critical temperature for producing higher-quality graphene with a larger $I_{2D/G}$ value.

By increasing the compression on the sample between the two electrodes, the conductivity of the carbon source increases, thus decreasing the discharge time (Fig. 2d, e, g). While maintaining the flash temperature between experimental runs at ~3,100 K, a short flash duration of 10 ms results in a higher 2D band, whereas a flash of 50–150 ms results in a lower 2D band product (Fig. 2g). This indicates that, given more time, the graphene flakes stack, orient and form more layers, lowering the 2D band of the resulting FG. A low cooling rate increases the flash duration and decreases the 2D band[22]. Therefore, to obtain a high $I_{2D/G}$, a thin quartz tube is chosen to accelerate the radiative cooling rate. Interestingly, although the internal temperatures exceed 3,000 K, the external walls of the quartz tubes are only warm to the touch (<60 °C) after the flash process. Most of the heat exits as black-body radiation.

X-ray photoelectron spectroscopy analysis shows a considerable reduction of elements other than carbon in FG and increases in the sp^2 carbon bond content (Supplementary Figs. 13, 14). Carbon has a

石墨化碳产生更大的石墨烯片(补充图7). C-FG的XRD分析显示, 除了26.0° 处的主峰(002)外, 2θ =42.5° 处的尖峰(100)与平面内原子间距有关(图1e). 在(100)峰的一半最大值处的窄的全宽度表明相对于由一些其他起始材料形成的FG, 较大的平面内片层尺寸. HR-TEM显示A-FG和C-FG中的折叠石墨烯片(图1e), 平均尺寸为0.5 μm和分别为1.2 μm(补充图7), 与通过石墨剥离获得的石墨烯片的尺寸相似. 这些样品上的选区电子衍射测量显示了单层和涡轮层石墨烯(补充图8-10.)

可使用其他富含、可再生或废物来源的碳, 如木炭、生物炭、腐殖酸、角蛋白(人头发、木质素、蔗糖、淀粉、松树皮、橄榄油烟灰、卷心菜、椰子、开心果壳、土豆皮、橡胶轮胎和混合塑料(补充图11, 补充表4), 包括聚对苯二甲酸乙二醇酯(PET或PETE)、高密度或低密度聚乙烯、聚氯乙烯、聚丙烯和聚丙烯腈. 当将合成聚合物转化为FG时, 非碳原子升华为小分子, 从而得到含碳量非常高的产物, 如图所示. 然而, 聚合物和橡胶解聚也可以保证提供在转化前升华的低聚物；因此, 使用热解产物更经济, 其中挥发物首先在工业上去除作为燃料源17, 残余碳转化为FG. 这在这里用橡胶轮胎衍生炭黑(补充图11, 补充表2, 4)进行了演示. 这些FG工艺都没有得到优化. 优化仅在CB-FG上执行, 如下所述. FJH工艺可以提供一个简单的途径将这些废物转化为潜在的高价值的FG

石墨烯I2D/G通过调整电极之间的样品压缩(这会影响样品导电性)、电容电压和开关持续时间来优化, 以控制闪光的温度和持续时间(图2a -g). 增加电压将提高工艺的温度. 通过将黑体辐射光谱拟合到600-1100纳米辐射中来估计温度(补充图12). 我们通过改变合成过程中的时间和温度, 利用低倍拉曼光谱(见方法)研究了CB-FG的质量. 在<90v和<3000k时, FG具有高D峰, 表明存在缺陷结构(图2a c, f). 通过提高电压输出, 在3100k下形成CB-FG, 其缺陷数量少, 拉曼光谱中几乎没有D带. 因此, 3000k是制备高质量、高I2D/G石墨烯的临界温度. 通过增加两个电极之间对样品的压缩, 碳源的导电性增加, 从而减少放电时间(图2d, e, g). 在将实验运行之间的闪蒸温度保持在~3100 K的同时, 10 ms的短闪蒸时间导致更高的2D带, 而50 -150 ms的闪蒸导致更低的2D带的产物(图2g). 这表明, 在更长的时间内, 石墨烯片堆叠、定向并形成更多的层, 从而降低生成的FG的2D带. 低冷却速率增加闪光持续时间并降低2D带. 因此, 为了获得高的I2D/G, 选择薄石英管来加速辐射冷却速率. 有趣的是, 尽管内部温度超过3000 K, 但石英管的外壁在闪蒸过程后仅能接触到温度(<60 ° C). 大部分热量以黑体辐射的形式排出.

X射线光电子能谱分析表明, FG中除碳以外的元素显著减少, sp2碳键含量增加(补充图. 碳有一个

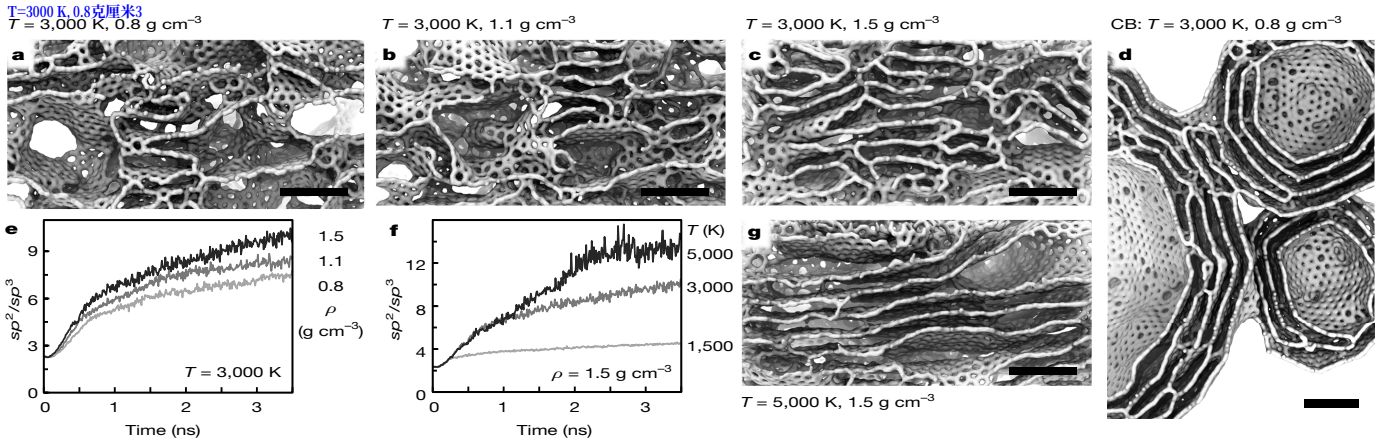

图3 | 分子动力学模拟. 各种结构
Fig. 3 | Molecular dynamics simulations. Structures with various
使用Nos-Hoover恒温器, 在给定的温度范围(1500至5000 K)下保持高达5×10 s的特性(如
characteristics (such as micro-porosity, misalignment and size of graphitic
微孔隙、错配和石墨畴的尺寸).
domains) kept at a given temperature range (1,500 to 5,000 K) for up to 5×10^{-9} s
a -c, 密度为0.8 g cm -3(a；海绵状结构)、1.1 g
with a Nosé–Hoover thermostat. **a**–**c**, Sample structures for carbon materials of
cm-3(b)和1.5 g cm-3(c；高度石墨化)的碳材料的样品结构, 在3000 K.d退火后, 炭黑
density 0.8 g cm^{-3} (**a**; sponge-like structure), 1.1 g cm^{-3} (**b**), and 1.5 g cm^{-3} (**c**; high
d退火后, 炭黑
degree of graphitization) after annealing at 3,000 K. **d**, Carbon black with
密度为0.8g cm 3, 大孔隙率, 在3600k下经过长时间(5×109s)退火, 可见多边形条
density 0.8 g cm^{-3} and large macro-porosity, after prolonged (5×10^{-9} s)
纹.
annealing at 3,600 K; polygonal fringes are apparent. **e**–**f**, Change of the
和不同温度T()退火时材料结构组成的变化.
structural composition of materials during annealing for materials of different
densities ρ (**e**) and for annealing at different temperatures T (**f**). **g**, Structure of
g,5000 K退火后
密度为1.5 g cm -3的材料的结构；初始结构与c所示相同.
material with density 1.5 g cm^{-3} after annealing at 5,000 K; the initial structure is
所有比例尺均为1.5nm.
the same as that shown in **c**. All scale bars are 1.5 nm.

高升华温度约3900 K；其他元素如铝或硅在<3000K时挥发。
high sublimation temperature of ~3,900 K; other elements such as
aluminium or silicon volatilize out at <3,000 K.

热重分析表明, FG产物比其来源的材料更具氧化稳定性(补充图15),
Thermogravimetric analysis in air shows that FG products are more
oxidatively stable than the materials from which they are derived (Sup-
比用Hummer s方法23获得的还原氧化石墨烯更稳定.
plementary Fig. 15) and more stable than reduced graphene oxide
在某些情况下, 会检测到氧化硅残留物,
obtained with Hummer's method[23]. In some cases, silicon oxide residues
这些残留物来自经过多次使用后磨损的石英管.
are detected, which come from worn out quartz tubes after multiples
uses.

先前的研究表明, 石墨烯可以在无催化剂的情况下在极高的温度下合成.
Previous studies have shown that graphene can be synthesized
然而, 当如图所
without catalysts at extremely high temperatures[24–26]. However, when
示优化FG时, 当控制反应时间和温度时, FG可以具有非常高的质量.
FG is optimized as shown here, it can have exceptionally high quality
此外, 电流可
when the reaction time and temperature are controlled. Furthermore,
以促进石墨烯的结晶.
the electric current can facilitate the crystallization of graphene[27].
在FJH过程中, 氢、氮和氧的脱气可能有助于在咖啡衍生的FG中形成大而薄的石墨烯片,
Degassing of hydrogen, nitrogen and oxygen during the FJH process
因为它可以防止石墨烯层的堆积, 从而允许进一步生长.
might contribute to the formation of large and thin graphene sheets
in coffee-derived FG because it could prevent stacking of graphene
layers, thereby permitting further growth[25,28,29].

为了评估FG快速生长的机理, 我们采用了大规模的AIREBO原子间势模拟,
To assess the mechanism of the rapid FG growth, we employ large-
如LAMMPS软件包(见方法)所实现的,
scale simulations with the AIREBO[30,31] interatomic potential as imple-
一些获得的结构如图3ad
mented in the LAMMPS package (see Methods)[32]. Some of the acquired
所示. 低密度材料在退火过程中产生海绵状结构
structures are shown in Fig. 3a–d. The low-density materials yield a
(图3a), 而密度增加导致石墨化程度高(图3c).
sponge-like structure (Fig. 3a) during annealing, whereas increased
我们注意到在
density leads to a high level of graphitization (Fig. 3c). We note the
低密度炭黑样品中石墨化程度很高, 其中显著增加的局部密度与高大孔隙率相结合(
high level of graphitization in the low-density CB sample, where the
图3d).
substantially increased local density is combined with high macro-
此外, 在模拟过程中, 退火过程通过sp2/sp3比率来定量化(图3e,f)。
porosity (Fig. 3d). Additionally, the annealing process is quantified
我们发现, 石墨烯的形
by the sp^2/sp^3 ratio during simulation (Fig. 3e, f). We find that the gra-
成过程在较低温度(<2000 K)下受到强烈损害, 但在较高温度(5000 K)下大大加速(图3g),
phene formation process is strongly impaired at lower temperatures
实验也表明了这一趋势(图2f).
(<2,000 K) but greatly accelerated at higher temperature (5,000 K)
在炭
(Fig. 3g)—a trend that is also suggested by experiments (Fig. 2f). In the
黑的情况下, FJH期间的连续缺陷愈合导致最初大致为球形的质心颗粒逐渐转变为多面体
case of carbon black, continuous defect healing during FJH results in
形状(图3d), 在透射电镜图像中以清晰的角度显示为条纹(见图1b, e), 进一步证实了所制备
the gradual conversion of initially roughly spherical centroid particles
材料的低缺陷性质.
into polyhedral shapes (Fig. 3d) that appear as fringes at clearly defined
angles in TEM images (see Fig. 1 b, e), further confirming the low-defect
nature of the produced materials.

通过增大石英管尺寸, 提高了FJH工艺的规模.
The FJH process was scaled up by increasing the quartz tube size. With
用直
径分别为4mm、8mm和15mm的石英管, 每批可分别合成30mg、120mg和1g的FG.
quartz tubes of 4 mm, 8 mm and 15 mm diameter, 30 mg, 120 mg and 1 g
图4a显示了使用三种管
of FG can be synthesized per batch, respectively. Figure 4a shows the
尺寸获得的CB-FG量. 从较小的管中产生
amount of CB-FG obtained with the three tube sizes. The shorter flash
的较短的闪光导致具有较高I2D/G的FG.
为了在保持成品质
from the smaller tube results in FG with a higher $I_{2D/G}$. To increase the
量的同时增加批量, 扁管很有帮助, 因为
batch size while maintaining FG quality, flat tubes are helpful because
they enable a higher cooling rate (Fig. 4a). For industrial production, we
对工业产品, 设想该过程可以自动进行连续FG合成(补充图16).
envision that the process can be automated for continuous FG synthesis
(Supplementary Fig. 16).

发现FG可分散于水/表面活性剂(Pluronic F-127)中, 使高浓度分散达到4 g l-1 (图4b,
FG was found to be dispersible in water/surfactant (Pluronic F-127)
补充图17).
to give highly concentrated dispersions reaching 4 g l^{-1} (Fig. 4b, Sup-
使用有机溶剂, FG具有高度的分散性(图4c)3335, 这可归因于
plementary Fig. 17). Using organic solvents, FG has a high degree of
允许有效剥离的涡轮层结构；层间吸引力远低于通过石墨剥离获得的传统排列的
dispersibility (Fig. 4c)[33–35], which can be attributed to the turbostratic
叠层石墨烯.
arrangement permitting efficient exfoliation; the interlayer attraction
forces are much lower than in conventionally arranged AB-stacked
graphene obtained by graphite exfoliation.

对FG复合材料进行了研究, 发现在较小的FG加入下, FG复合材料的物理性能显著
FG composites were explored, revealing considerably enhanced
提高.
含0.05%FG并固化28天的CB-FG水泥
physical properties at small FG loadings. CB-FG–cement composites
复合材料的抗压强度比不含FG的对照样品高出约25%(补充图18).
with 0.05% FG and cured for 28 days had ~25% higher compressive
strength than the FG-free control sample (Supplementary Fig. 18).
这种抗压强度的提高是最近报道的具有相同石墨烯负载的电化学剥离石墨烯增强水泥
This enhancement in the compressive strength is three times higher
复合材料的三倍, 并且略大于其他水泥石墨烯复合材料36,37.
than the values reported recently for cement composites reinforced
by electrochemically exfoliated graphene with the same graphene
loading, and slightly larger than those of other cement–graphene
composites[36,37]. The seven-day compressive and tensile strength of
含0.1%FG的CB-FG水泥复合材料的7天抗压强度和抗拉强度分别比
CB-FG–cement composites with 0.1% FG loading are ~35% and ~19%
不含FG的对照样品高35%和19%(图4d).
higher, respectively, than those of the FG-free control sample (Fig. 4d).
这些增强几乎是其他报道的石墨烯水泥复合材料在相同加入量下的三倍, 显示出快速的
These enhancements are almost three times larger than those of
强度提高。
other reported graphene–cement composites with the same load-
CB-FG水泥复合材料的
ing, demonstrating rapid strength development. Scanning electron
扫描电子显微镜图像(补充图19)显示了FG在水泥基体中的均匀分布.
microscopy images of CB-FG–cement composites (Supplementary
Fig. 19) show a homogeneous distribution of FG in the cement matrix.
CB-FG水泥复合材料的性能大大提高, 强度迅速提高, 这再次归因于涡轮层CB-FG的高
The largely enhanced properties and rapid strength development of
分散性, 这导致了更均匀和更坚固的复合材料(更多解释见补充信息).
CB-FG–cement composites is again attributed to the high dispers-
ibility of the turbostratic CB-FG, which results in greater homogeneity
and robust composites (see Supplementary Information for further
explanations).

此外, CB-FG有效地提高了聚合物的性能.
In addition, CB-FG effectively enhances polymer properties. A
0.1 wt%CB-FG聚二甲基硅氧烷(PDMS)复合材料的抗压强度比不含石墨烯的PDMS提高了
0.1wt% CB-FG–polydimethylsiloxane (PDMS) composite showed ~250%
约250%(补充图20).
increase in compressive strength compared with PDMS without gra-
phene (Supplementary Fig. 20).

为了证明其在电化学储能装置中的适用性, 还将C-FG和CPC-FG用作锂离子电容器和
To demonstrate its applicability in electrochemical energy storage
锂离子电池中的电极材料(补充图21), 展示了在高级能源应用中使用FG的潜力.
devices, C-FG and CPC- FG were also used as electrode materials in a
Li-ion capacitor and a Li-ion battery (Supplementary Fig. 21), dem-
onstrating the potential to use FG in advanced energy applications.

总之, 从超低成本碳源(如煤和石油焦)、可再生资源(如生物炭)出发, 采用自下
In summary, a low-energy bottom-up synthesis of easily exfoliated tur-
而上的低能耗方法合成了易剥落的涡轮层状石墨烯
bostratic graphene was demonstrated from ultralow-cost carbon sources
(such as coal and petroleum coke), renewable resources (such as biochar
and rubber tyres) and mixed-waste products (including plastic bottles

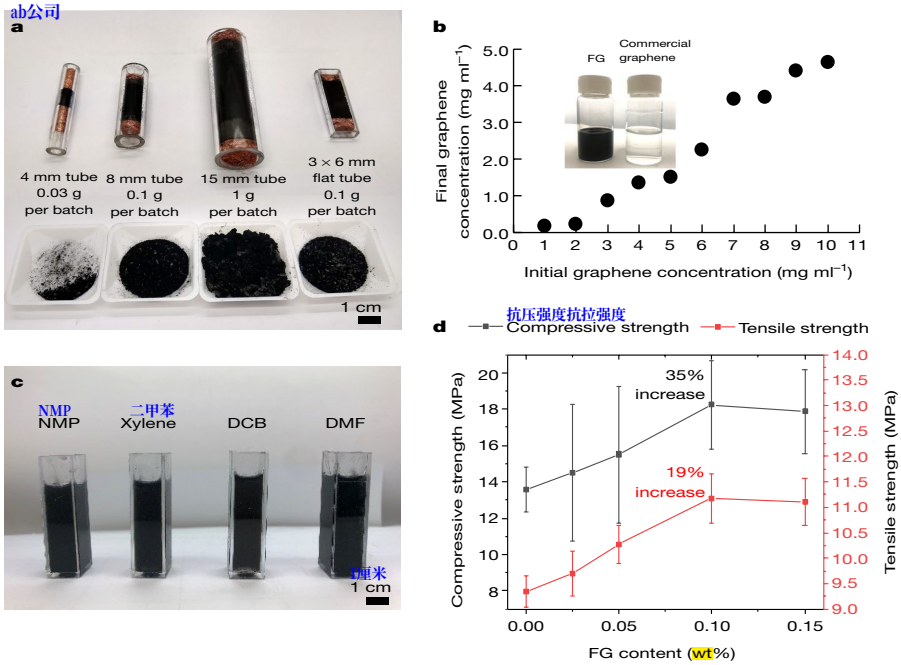

图4:CB-FG的放大和应用. a. 不同尺寸和形状, FJH石英管用于合成FG

Fig. 4 | Scaling up and applications of CB-FG. a, FJH quartz tubes of different sizes and shapes, used to synthesize FG. Two separate synthesis processes were conducted with each tube, providing the samples in the tube and those in the plastic dishes. **b**, FG dispersion in a water–Pluronic (F-127) solution (1%). The photograph shows the supernatants of 4 g l^{-1} and of CB-FG and of 10 g l^{-1} of a commercial sample after centrifugation. The commercial graphene was not stable as a colloid at this concentration, resulting in a clear liquid in the supernatant after centrifugation. **c**, FG dispersion in various organic solvents at 5 g l^{-1}. **d**, Mechanical performance of cement compounded with FG. The error bars represent one standard error ($n = 3$).

每根试管分别进行两个合成过程, 提供试管中的样品和塑料皿中的样品. 照片显示了离心后CB-FG的4 g l−1和商业样品的10 g l−1的上清液. 在这个浓度下, 商用石墨烯为不稳定为胶体, 因此离心后上清液中是一种清澈的液体. b.FG在水Pluronic(F-127)溶液(1%)中的分散. c.FG在不同有机溶剂中以5g l−1分散. d.FG复合水泥的力学性能. 误差条表示一个标准误差(n=3).

以及丢弃的食物). 放大的FG合成工艺可以为大块结构复合材料提供涡轮层状石墨烯. and discarded food). Scaling up of the FG synthesis process could provide turbostratic graphene for bulk construction composite materials.

Online content

Any methods, additional references, Nature Research reporting summaries, source data, extended data, supplementary information, acknowledgements, peer review information; details of author contributions and competing interests; and statements of data and code availability are available at https://doi.org/10.1038/s41586-020-1938-0.

一.Allen, M.J., Tung, V.C.和Kaner, R.B.《蜂窝碳：石墨烯评论》. 化学.
1. Allen, M. J., Tung, V. C. & Kaner, R. B. Honeycomb carbon: a review of graphene. *Chem. Rev.* **110**, 132–145 (2010). 修订版,110132145(2010年).

2.Yi, M.和Shen, Z. 机械去角质技术在规模化生产中的应用
2. Yi, M. & Shen, Z. A review on mechanical exfoliation for the scalable production of graphene. *J. Mater. Chem. A* **3**, 11700–11715 (2015). 石墨烯. J.马特. 化学.

三.Hernandez, Y.等人. 液相剥离法剥落石墨烯
3. Hernandez, Y. et al. High-yield production of graphene by liquid-phase exfoliation of graphite. *Nat. Nanotechnol.* **3**, 563–568 (2008). 纳特. 纳米技术.

四.Eda, G., Fanchini, G.和Chhowalla, M.作为透明和柔性电子材料的还原氧化石墨烯大面积超薄薄膜.
4. Eda, G., Fanchini, G. & Chhowalla, M. Large-area ultrathin films of reduced graphene oxide as a transparent and flexible electronic material. *Nat. Nanotechnol.* **3**, 270–274 (2008).

5个.Li, D.等人. 石墨烯纳米片的可加工水分散体. 纳特. 纳米技术.
5. Li, D. et al. Processable aqueous dispersions of graphene nanosheets. *Nat. Nanotechnol.* **3**, 101–105 (2008).

6.Lin, L., Peng, H.和Liu, Z.《石墨烯工业的合成挑战》. 纳特. 马特.
6. Lin, L., Peng, H. & Liu, Z. Synthesis challenges for graphene industry. *Nat. Mater.* **18**, 520–524 (2019).

7号.法拉利, A.C.等. 石墨烯和石墨烯层的拉曼光谱. 菲斯.修订版.利特.97年.
7. Ferrari, A. C. et al. Raman spectrum of graphene and graphene layers. *Phys. Rev. Lett.* **97**, 187401 (2006).

8个.法拉利, 石墨烯和石墨的拉曼光谱：无序, 电子声子
8. Ferrari, A. C. Raman spectroscopy of graphene and graphite: disorder, electron–phonon coupling, doping and nonadiabatic effects. *Solid State Commun.* **143**, 47–57 (2007). 耦合、掺杂和非绝热效应. 固态公社.

9号.Malard, L.M., Pimenta, M.A., Dresselhaus, G.&Dresselhaus, M.S.石墨烯的拉曼光谱.
9. Malard, L. M., Pimenta, M. A., Dresselhaus, G. & Dresselhaus, M. S. Raman spectroscopy in graphene. *Phys. Rep.* **473**, 51–87 (2009). 菲斯.报告473, 51至87(2009).

10个.Ni, Z.H.等人. 用拉曼光谱探测悬浮石墨烯中的带电杂质
10. Ni, Z. H. et al. Probing charged impurities in suspended graphene using Raman spectroscopy. *ACS Nano* **3**, 569–574 (2009). 光谱学. ACS纳米356957.4(2009).

11号.加洛, J.A.等人. Ni(111)上涡轮层状石墨烯的大面积物理生长
11. Garlow, J. A. et al. Large-area growth of turbostratic graphene on Ni (111) via physical vapor deposition. *Sci. Rep.* **6**, 19804 (2016). 气相沉积. 科学.报告619804(2016).

12岁.Niilisk, A.等人. 探测多层石墨烯层和的拉曼光谱表征.
12. Niilisk, A. et al. Raman characterization of stacking in multi-layer graphene grown on Ni. *Carbon* **98**, 658–665 (2016). 碳98658665(2016).

13岁.Li, Z.Q.等人. 石墨和涡轮碳的X射线衍射图.
13. Li, Z. Q. et al. X-ray diffraction patterns of graphite and turbostratic carbon. *Carbon* **45**, 1686–1695 (2007). 碳45.

14岁.富兰克林, R.E.石墨化和非石墨化碳中的微晶生长.
14. Franklin, R. E. Crystallite growth in graphitizing and non-graphitizing carbons. *Proc. R. Soc. Lond.* **209**, 196–218 (1951). 过程. 社会福利.隆德.

15岁.斯坦科维奇, S.等人. 化学还原法剥备石墨烯基纳米片
15. Stankovich, S. et al. Synthesis of graphene-based nanosheets via chemical reduction of exfoliated graphite oxide. *Carbon* **45**, 1558–1565 (2007). 剥落的氧化石墨. 碳45.1558.1565(2007).

16岁.Cai, M., Thorpe, D., Adamson, D.H.和Schniepp, H.C.石墨剥落.方法.
16. Cai, M., Thorpe, D., Adamson, D. H. & Schniepp, H. C. Methods of graphite exfoliation. *J. Mater. Chem.* **22**, 24992–25002 (2012).

17岁.Miandad, R.等人. 塑料废弃物的催化热解：向热解生物精炼方向发展.
17. Miandad, R. et al. Catalytic pyrolysis of plastic waste: moving toward pyrolysis based biorefineries. *Front. Energy Res.* **7**, 27 (2019). 前面. 能源研究7, 27(2019).

18岁.吉布, 不可降解化比亚省. 塑料永远是. 纳特. 化学.1139405(2019年).
18. Gibb, B. C. Plastics are forever. *Nat. Chem.* **11**, 394–395 (2019).

19岁.Parfitt, J., Barthel, M.和Macnaughton, S.《食品供应链中的食品废物：量化和到2050年的变化潜力》.
19. Parfitt, J., Barthel, M. & Macnaughton, S. Food waste within food supply chains: quantification and potential for change to 2050. *Philos. Trans. R. Soc. B* **365**, 3065–3081 (2010). 菲洛斯. 事务处理.社会福利.B 365, 3065 3081(2010年).

20岁.Gustavsson, J., Cederberg, C., Sonesson, U., van Otterdijk, R. & Meybeck, A. *Global Food Losses and Food Waste: Extent, Causes and Prevention* (FAO, 2011); http://www.fao.org/3/a-i2697e.pdf.
20. Gustavsson, J., Cederberg, C., Sonesson, U., van Otterdijk, R. & Meybeck, A. *Global Food* 损失和食物浪费：程度、原因和预防(粮农组织, 2011年)；http://www.FAO.org/3/

21岁.Jambeck, J.R.等人. 塑料废物从陆地输入海洋. 科学34776871
21. Jambeck, J. R. et al. Plastic waste inputs from land into the ocean. *Science* **347**, 768–771 (2015).

22岁.Yao, Y.等人. 碳热冲击法合成高熵合金纳米粒子. 科学类
22. Yao, Y. et al. Carbothermal shock synthesis of high-entropy-alloy nanoparticles. *Science* **359**, 1489–1494 (2018).

23岁.Advincula, P.A.等人. 通过将相变材料封装在碳纳米颗粒中来调节体积变化和传递热导率.
23. Advincula, P. A. et al. Accommodating volume change and imparting thermal conductivity by encapsulation of phase change materials in carbon nanoparticles. *J. Mater. Chem. A* **6**, 2461–2467 (2018). J.马特. 化学.

24岁.查克拉巴蒂, A.等人. 二氧化碳转化为几层石墨烯. J.马特. 化学
24. Chakrabarti, A. et al. Conversion of carbon dioxide to few-layer graphene. *J. Mater. Chem.* **21**, 9491–9493 (2011). 219.019493(2011年).

25岁.林, J.等. 激光诱导商业聚合物多孔石墨烯薄膜. 纳特.
25. Lin, J. et al. Laser-induced porous graphene films from commercial polymers. *Nat. Commun.* **5**, 5714 (2014). 公社.

26岁.Nepal, A., Singh, G.P., Flanders, B.N.和Sorensen, C.M.通过无催化剂气相碳氢化合物爆轰一步合
26. Nepal, A., Singh, G. P., Flanders, B. N. & Sorensen, C. M. One-step synthesis of graphene via catalyst-free gas-phase hydrocarbon detonation. *Nanotechnology* **24**, 245602 (2013). 成石墨烯. 纳米技术24245602(2013).

27岁.Huang, J.Y.等人. 高偏压焦耳加热下非晶碳纳米线微管形成的实时观察.
27. Huang, J. Y. et al. Real-time observation of tubule formation from amorphous carbon nanowires under high-bias Joule heating. *Nano Lett.* **6**, 1699–1705 (2006). 纳诺.莱特.61699.1705(2006).

28岁.哈里斯, P.J.F.电工程碳材料. 碳122504513(2017).
28. Harris, P. J. F. Engineering carbon materials with electricity. *Carbon* **122**, 504–513 (2017).

29岁.Luong, D.X.等人. 激光诱导石墨烯纤维. 碳126 472 479(2017).
29. Luong, D. X. et al. Laser-induced graphene fibers. *Carbon* **126**, 472–479 (2017).

30岁.斯图尔特, S.J.图坦, A.B.和哈里森, J.A. 分子间相互作用的碳氢化合物的反应势.
30. Stuart, S. J., Tutein, A. B. & Harrison, J. A. A reactive potential for hydrocarbons with intermolecular interactions. *J. Chem. Phys.* **112**, 6472–6486 (2000). J.化学.菲斯.112647.26486(2000年).

31岁.布伦纳, D.W.等人. 碳氢化合物的第二代反应经验键序势能表达式.
31. Brenner, D. W. et al. A second-generation reactive empirical bond order (REBO) potential energy expression for hydrocarbons. *J. Phys. Condens. Matter* **14**, 783–802 (2002). J.菲斯.康登斯. 问题14783802(2002).

32岁.短程分子动力学的快速并行算法. J.计算.
32. Plimpton, S. Fast parallel algorithms for short-range molecular dynamics. *J. Comput. Phys.* **117**, 1–19 (1995). 菲斯.117, 119(1995年).

33岁.Xu, Y.等人. 石墨烯液相剥离：剥离介质、技术和挑战综述.
33. Xu, Y. et al. Liquid-phase exfoliation of graphene: an overview on exfoliation media, techniques, and challenges. *Nanomaterials* **8**, 942 (2018). 纳米材料8942(2018).

34岁.O'Neill, A., Khan, U., Nirmalraj, P.N., Boland, J.和Coleman, J.N.石墨烯在低沸点溶剂中的分
34. O'Neill, A., Khan, U., Nirmalraj, P. N., Boland, J. & Coleman, J. N. Graphene dispersion and exfoliation in low boiling point solvents. *J. Phys. Chem. C* **115**, 5422–5428 (2011). 散和剥离. J.菲斯.化学.C 1155422428(2011年).

35岁.Dong, L.等人. 一种大规模生产超高浓度石墨烯浆料的非分散策略.
35. Dong, L. et al. A non-dispersion strategy for large-scale production of ultra-high concentration graphene slurries in water. *Nat. Commun.* **9**, 76 (2018). 纳特. 公社.

36岁.刘建军, 李建华, 徐旭, S.石墨烯和氧化石墨烯片材对水泥基材料的增强机理.
36. Liu, J., Li, Q. & Xu, S. Reinforcing mechanism of graphene and graphene oxide sheets on cement-based materials. *J. Mater. Civ. Eng.* **31**, 04019014 (2019). J.马特. 公民. 工程.

37岁.Krystek, M.等人. 高性能石墨烯基胶凝复合材料.
37. Krystek, M. et al. High-performance graphene-based cementitious composites. *Adv. Sci.* **6**, 1801195 (2019). .61801195(2019年).

Article

方法
Methods

FJH系统
FJH system

FJH的设置详见补充图1.
The FJH set up is detailed in Supplementary Fig. 1. Inside a quartz tube, two loosely fitting electrodes compress the carbon source using two copper-wool plugs or graphite spacers to contact the carbon sources to allow degassing of volatile materials. The compressing force is controllable by a modified small vice so as to minimize the sample resistance to 1–1,000 Ω, and is key to obtaining a good flash reaction (0.004–4 S cm^{-1}). To control the discharge time, a mechanical relay with programmable millisecond-level delay time is used. The entire sample reaction chamber is placed inside a low-pressure container (plastic vacuum desiccator) for safety and to facilitate degassing. However, the FJH process works equally well at 1 atm. The capacitor bank consists of 20 capacitors with a total capacitance of 0.22 F. Each capacitor is connected to the main power cable (or bus) by a circuit breaker that is also used as a switch to enable/disable each capacitor. The capacitor bank is charged by a d.c. supply capable of reaching 400 V. The first prototype system is placed conveniently on one plastic mobile cart (Supplementary Fig. 1b). Using a large 15-mm-diameter quartz tube, we achieve synthesis of 1 g of FG per batch using the FJH process.

在石英管内, 两个松散的棉塞或石墨垫片压缩碳源, 以接触碳源, 从而使挥发性物质脱气.
压缩力可以通过一个改进的小虎钳来控制, 从而将样品电阻降至1-1000Ω, 这是获得良好的闪光反应(0.004 -4 S cm-1)的关键.
为了控制放电时间, 采用了具有可编程毫秒级延迟时间的机械继电器.
整个样品反应室放置在低压容器(塑料真空干燥器)内, 以确保安全并便于脱气.
然而, FJH过程在1个atm下同样有效.
电容器组由20个电容器组成, 总电容为0.22F.
每个电容器通过断路器连接到主电缆(或总线), 断路器也用作开关, 以启用/禁用每个电容器.
电容器组由直流电源电压可达到400伏.
第一个原型系统方便地放置在一个塑料移动推车上(补充图1b).
使用直径为15 mm的大石英管, 我们使用FJH工艺实现了每批1 g FG的合成.
我们采取了以下措施来保护操作员和电路, 我们强烈建议采取这些措施.
电路的细节可以在补充图1a中找到.
在放电闪光过程中, 应佩戴深色安全眼镜, 以保护眼睛免受强光照射.

安全注意事项：电容器组能够产生致命的电脉冲.
Safety notice: the capacitor bank is capable of generating fatal electric pulses. Therefore, the following steps are taken to protect the operator as well as the circuit, and we strongly suggest that these measures be followed. Details of the circuit can be found in Supplementary Fig. 1a. Darkened safety glasses should be worn to protect eyes from the bright light during the discharge flashing process.

断路器的电压和电流额定值适用于每个电容器在50-200 ms放电时间基础上向FJH
The voltage and current ratings for the circuit breaker are appropriate for the maximum voltage and the anticipated maximum current that will be supplied by each capacitor to the FJH discharge on the basis of a discharge time of 50–200 ms. We use the maximum charging and bleeding voltages at ~400 V with maximum currents of 0.7 A and 0.1 A, respectively. The pulse discharging voltage to the sample is ~400 V and current can reach up to 1,000 A in <100 ms. A 24-mH inductor is used to avoid current spikes while using the mechanical relay. Without the inductor, the mechanical relay could be prone to high-current arcing during the intermittent closing of the circuit. To protect the inductor from the spike voltage when shutting off the current, a diode and a low-resistance resistor with appropriate ratings are connected parallel to the inductor. Additionally, to protect the capacitor from reverse polarity in case of oscillatory decay (which can occur in a fast discharge), an appropriate diode is placed parallel to the capacitor bank.

放电提供的最大电压和预期最大电流.
我们使用的最大充电和放电电压约为400v,
样品的脉冲放电电压约为400v, 电流在100ms内可达1000A.
使用机械继电器时, 使用24 mH电感以避免电流尖峰.
没有电感器,
机械继电器在电路间歇闭合时容易产生大电流电弧.
为了在切断电流时保护电感器不受尖峰电压的影响, 一个二极管和一个具有适当额定值的低电阻电阻器并联在电感器上.
此外, 为了在振荡衰减(在快速放电中可能发生)的情况下保护电容器不受反极性的影响, 特适当的二极管平行于电容器组放置.

表征
Characterization

利用FEI-Helios纳米实验室660双光束扫描电镜系统, 在5kv下, 在10mm的工作距离下, 用扫描电子显微镜(SEM)对合成的FG产品进行了表征.
The resultant FG products were characterized by scanning electron microscopy (SEM) using an FEI Helios NanoLab 660 DualBeam SEM system at 5 kV with a working distance of 10 mm. X-ray photoelectron spectroscopy (XPS) data were collected with a PHI Quantera SXM Scanning X-ray Microprobe with a base pressure of 5×10^{-9} torr. Survey spectra were recorded using 0.5-eV steps with a pass energy of 140 eV. Elemental spectra were recorded using 0.1-eV steps with a pass energy of 26 eV. All of the XPS spectra were corrected using the C 1*s* peak (284.5 eV) as reference.

采用PHI-Quantera-SXM扫描X射线微探针, 在5×10-9torr的基底压力下, 收集了X射线光电子能谱(XPS)数据.
测量光谱用0.5-eV台阶记录, 通过能量为140eV
用0.1ev台阶记录元素光谱, 通过能为26ev.
以C 1s峰(284.5ev)为参考, 对所有XPS谱进行了校正.
用JEOL 2100F场发射枪TEM在200kv下拍摄TEM图像.
TEM images were taken with a JEOL 2100F field-emission gun TEM at 200 kV. Atomic-resolution HR-TEM images were taken with an FEI Titan Themis S/TEM system at 80 keV. Samples were prepared by dropping diluted dispersions (~1 mg ml^{-1} in isopropanol) of the graphene sample (<200 µl) on the TEM Cu grids. The dispersion was prepared using a bath sonicator (~15 min). Electron diffraction was calibrated by a diffraction standard (evaporated Al grid; Ted Pella).

在80 keV 下, 用FEI-Titan-Themis S/TEM系统拍摄了高分辨高分辨透射电镜图像.
通过将石墨烯样品(<200 l)的稀释分散液(
异丙醇中约1 mg ml 1)滴入TEM-Cu网格上制备样品.
使用浴式超声波仪(约15分钟)制备分散液,
电子衍射用衍射标准校准(蒸发铝栅；特德佩拉).
在暴露于溶剂之前, 使用Renishaw拉曼显微镜和功率为5mw的532nm激光, 将制备好的FG样品置于玻片上收集所有拉曼光谱.
All Raman spectra were collected with as-prepared FG samples atop a glass slide, before exposure to solvent, using a Renishaw Raman microscope and a 532-nm laser with a power of 5 mW. A 50× lens was used for the local Raman spectra in Fig. 1 and a 5× lens for the mean Raman spectra in Fig. 2.

图1中的局部拉曼光谱使用50×透镜, 平均拉曼光谱使用5×透镜

原子模拟
Atomistic modelling

除了含有55000个原子的炭黑模型外, 所有结构均采用周期性边界条件进行原子模拟,
每个晶胞约有15000个原子.
Atomistic simulations were carried out using periodic boundary conditions with ~15,000 atoms per unit cell for all structures except the carbon black model, which contained ~55,000 atoms.
初始结构是由任意形状、直径高达812的石墨薄片的随机定位和错误定向, 然后添加随机定位的单个碳原子(原子碳含量约为50%, 代表源材料的非石墨化部分)形成的.
The initial configurations were created by random positioning and misorientation of small graphitic flakes of arbitrary shape and up to 8–12 Å in diameter, and subsequently adding randomly positioned individual carbon atoms (the atomic carbon content was ~50% to represent a non-graphitized portion of the source material). Carbon black centroid particles were created by arranging randomly oriented graphitic flakes in roughly spherical shapes with hollow cores and diameters of up to 12 nm, and adding atomic carbon (~50%). The initial configurations were subjected to preliminary annealing at 400 K for 2×10^{-9} s to eliminate irregularities caused by the structure creation protocol, then heated to the target annealing temperature with a heating speed of 0.5×10^{-12} K s^{-1} using a Nose–Hoover thermostat (canonical NVT ensemble) with a temperature damping parameter of 0.025×10^{-12} s. The structures were held at the target annealing temperatures for 5×10^{-9} s (15×10^{-9} s for carbon black).

初始结构在400 K下进行2×10 -9 s的预退火, 以消除由结构生成方式引起的不规则, 然后使用具有温度阻尼的Nose-Hoover恒温器(典型NVT系综)以0.5×10 -12 K s -1的加热速度加热到目标退火温度参数为0.025×10-12s
结构在目标退火温度下保持5×10-9s(炭黑为15×10-9s).

水溶液中闪蒸石墨烯分散体的制备
Preparation of flash graphene dispersion in water–Pluronic solution

将FG分散于浓度为110g | -1的水溶液(F-127)(1%)中.
FG was dispersed in water–Pluronic (F-127) solution (1%) at concentrations of 1–10 g l^{-1}. The mixture was sonicated in an ultrasonic bath for 40 min to obtain a dark dispersion. The dispersion was subjected to centrifugation at 1,500 rpm (470 relative centrifugal force) for 30 min to remove aggregates using a Beckman Coulter Allegra X-12 centrifuge equipped with a 19-cm-radius rotor. The supernatant was analysed via ultraviolet–visible spectroscopy (Shimadzu). The dispersions were diluted 500 times and the absorbance was recorded at 660 nm. An extinction coefficient of α_{660} = 6,600 l g^{-1} m^{-1} was used to calculate the concentration of graphene in the solution.

将混合物在超声波浴中超声处理40分钟以获得暗分散体.
将分散液以1500转/分钟离心力)离心30分钟, 使用配有19厘米半径转子的贝克曼库尔特-阿莱格拉X-12离心机去除聚集块.
上清液用紫外可见光谱法(岛津)分析.
将分散液稀释500倍, 在660nm处记录吸光度,
用消光系数 α 660=6600 l g -1 m-1 计算溶液中石墨烯的浓度.

水泥样品制备
Cement sample preparation

将不同浓度的FG分散在1%水溶液中.
FG at various concentrations was dispersed in 1% water–Pluronic (F-127) solution. The dispersion was agitated for 15 min at 5,000 rpm using a shear mixer (Silverson L5MA). The graphene suspension in water was mixed with Portland cement with a water-to-cement ratio of 0.40. The slurry was cast in 5 × 5 × 5 cm^3 cubic polytetrafluoroethylene moulds (for compressive strength measurements) and in 2.5 cm × 3.8 cm cylindrical moulds (for tensile strength measurements). All cubes and cylinders were taken out the moulds after 24 h and placed in water for curing for another 24 h. The compressive and tensile mechanical strengths were measured after 7 and 28 days. For each FG–cement ratio, three samples were cast and tested.

使用剪切混合器(Silverson L5MA)以5000 rpm搅拌分散液15分钟,
将石墨烯悬浮液与水灰比为0.40的硅酸盐水泥混合.
将泥浆浇铸在5×5×5cm3的立方体聚四氟乙烯模具(用于抗压强度测量)和2.5cm×3.8cm圆柱形模具(用于抗拉强度测量)中.
24小时后取出所有立方体和圆柱体, 放入水中养护24小时.
第7天和第28天测量抗压和抗拉机械强度.
对于每种FG水泥比, 浇铸并测试三个样品.

水泥和PDMS测试程序
Cement and PDMS testing procedures

抗压强度.
Compressive strength. The compression strength tests were performed using a Forney Variable Frequency Drive automatic machine with dual load cells for maximum accuracy.

抗压强度试验是使用具有双测力传感器的Forney变频驱动自动机器进行的, 以获得最大精度.

抗拉强度.
Tensile strength. Owing to the brittle nature of cement-based materials, the tensile strength was calculated via a splitting test because it gives the most accurate measurement. Special jigs held the cylinders so that the uniaxial compressive force applied to the centre lines of the bottom and top surfaces of the samples caused tensile stress between the points of contact.

由于水泥基材料的脆性, 其抗拉强度是通过劈裂试验计算出来的, 因为劈裂试验给出了最精确的测量结果.
特殊的夹具固定住圆柱体, 使施加在样品底部和顶部中心线上的单轴压缩力在接触点之间产生拉应力,

数据可用性
Data availability

在当前研究中生成和/或分析的数据集有
The datasets generated and/or analysed during the current study are available from the corresponding author on reasonable request.

感谢G.A.Lopez Silva准备FJH工艺示意图, J.Li准备橄榄油烟尘, Oxbow煅烧国际有限责任公司捐赠煅烧
Acknowledgements We thank G. A. Lopez Silva for preparing the schematic of the FJH
焦炭, Ergon沥青和乳化液公司捐赠橡胶轮胎衍生炭黑, Nerval有限责任公司捐赠生物炭.
process, J. Li for preparing the olive oil soot, Oxbow Calcining International LLC for donating
the calcined coke, Ergon Asphalt and Emulsions, Inc. for donating the rubber-tyre-derived
K.V.B.和B.I.Y.感谢美国国家科学基金会
carbon black, and Neroval LLC for donating the biochar. K.V.B. and B.I.Y. thank the National
(NSF)的支持(CBET-1605848)和美国能源部的B.Sastri的讨论.
Science Foundation (NSF) for support (CBET-1605848) and B. Sastri of the US Department of
R.感谢NSF-DMR 1709051的部分支持.J.M.T.感谢美国空军科学研究办公室
Energy for discussions. R.S. thanks the partial support of NSF-DMR 1709051. J.M.T. thanks the
(FA9550-19-1-0296)的支持.
US Air Force Office of Scientific Research (FA9550-19-1-0296) for support.

作者贡献了D.X.L.发现了碳材料向石墨烯的FJH转化, 设计和建造了FJH装置, 设计和建造了用于温度测定的光谱仪
Author contributions D.X.L. discovered the FJH conversion of carbon materials to graphene,
, 获得了大部分数据, 并撰写了大部分手稿.
designed and built the FJH apparatus, designed and built the spectrometer for temperature
K.V.B.在
determination, acquired most of the data, and wrote most of the manuscript. K.V.B. conducted
B.I.Y.W.A.A.和P.A.A.的指导下进行了力学理论计算, 制作了一些FG样品, 并对聚合物混合物进行了共混和测试
the mechanistic theory calculations under the guidance of B.I.Y. W.A.A. and P.A.A. fabricated
M.G.S.获得了扫描电镜图像.
some FG samples, and blended and tested the polymer blends. M.G.S. obtained the SEM
并写下了部分补充信息, 特别是关于FG形态的信息.
images and wrote parts of Supplementary Information, especially regarding FG morphology.
C.K.协助设计FG仪器和光谱仪, 并编写了
C.K. assisted with the design of the FG apparatus and the spectrometer, and wrote parts of
关于涡轮层石墨烯的补充信息.
Supplementary Information regarding turbostratic graphene. R.V.S. obtained most of the TEM
R.V.S.获得了大部分TEM图像和所有选
定区域的电子衍射数据.
W.C.和H.G.获得了一些TEM图像.
images and all of the selected-area electron diffraction data. W.C. and H.G. obtained some of
M.建造并测试了锂离子电容器.
C.K.和V.M.协助D.X.L.完成FJH系统的
the TEM images. M.R. built and tested the lithium-ion capacitor. C.K. and V.M. assisted D.X.L. in
设计和安全功能.
E.A.M.进行热重分析.
the design and safety features of the FJH system. E.A.M. performed the thermogravimetric
Z.得到了表面积.
M.B.获得水泥和聚合物复合材料
analysis. Z.W. obtained the surface area. M.B. obtained the cement and polymer composite
R.S.指导下的数据.
这项研究的各个方面都由J.M.T.监督, J.M.T.负责抄写手稿的一些章节.
data under the guidance of R.S. All aspects of the research were overseen by J.M.T., who co-
wrote some sections of the manuscript.

FG合成过程是水稻大学的知识产权.
Competing interests The FG synthesis process is the intellectual property of Rice University.
J.M.T., D.X.L.和V.M.将成为Universal Matter有限公司的股东, 该公司授权莱斯大学的FG知识产权, 并扩大这
J.M.T., D.X.L. and V.M. will be stockholders in Universal Matter Ltd, a company licensing the FG
一过程.
在撰写和提交本手稿时, 普遍
intellectual property of Rice University and scaling up this process. At the time of the writing
事项许可证尚未完善.
and submission of this manuscript, the license to Universal Matter has not been consummated.
C-Crete技术拥有石墨烯水泥/混凝土复合材料加固的知识产权.
C-Crete Technologies owns intellectual property on the strengthening of graphene–cement/
九.M.现在被宇宙物质所利用,
D.X.L.和J.M.T.将继续在莱斯大学
concrete composites. V.M. is now employed by Universal Matter. D.X.L. and J.M.T. will remain
全职工作, 而D.X.L.可能在两年内被环球公司聘用.
full time with Rice University, whereas D.X.L. might be employed by Universal Matter in two
J.M.T.和D.X.L.的所有利益冲突均通过定期向莱斯大学赞助项目和研究合规办公室披露进行管理.
years. All conflicts of interest for J.M.T. and D.X.L. are managed through regular disclosure to
the Rice University Office of Sponsored Programs and Research Compliance.

附加信息
Additional information
本文的补充信息见https://doi.org/10.1038/s41586-020-
Supplementary information is available for this paper at https://doi.org/10.1038/s41586-020-
1938-0.
应向R.S., B.I.Y.或J.M.T.发送信函和材料请求.同行评审信息性质感谢Loh Kian Ping和其他匿名评审员
Correspondence and requests for materials should be addressed to R.S., B.I.Y. or J.M.T.
对本工作的同行评审做出的贡献.
Peer review information *Nature* thanks Loh Kian Ping and the other, anonymous, reviewer(s)
for their contribution to the peer review of this work.
重印和许可信息可在http://www.nature.com/Reprints上获得.
Reprints and permissions information is available at http://www.nature.com/reprints.